NASA TN D-266

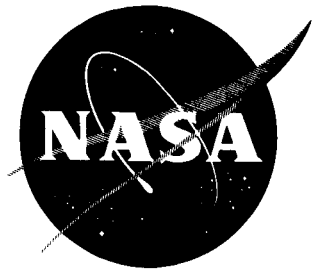

TECHNICAL NOTE

D-266

ANALYSIS OF ONE-DIMENSIONAL ION ROCKET WITH GRID NEUTRALIZATION

By Harold Mirels and Burt M. Rosenbaum

Lewis Research Center
Cleveland, Ohio

NATIONAL AERONAUTICS AND SPACE ADMINISTRATION

WASHINGTON March 1960

CONTENTS

NATIONAL AERONAUTICS AND SPACE ADMINISTRATION

TECHNICAL NOTE D-266

ANALYSIS OF ONE-DIMENSIONAL ION ROCKET WITH GRID NEUTRALIZATION

By Harold Mirels and Burt M. Rosenbaum

SUMMARY

A one-dimensional analysis is made of an ion rocket employing three grids. The first grid emits ions, the second accelerates the ions to a velocity beyond the desired final value, and the third decelerates the ions to the desired final velocity and neutralizes them by the emission of electrons. The analysis neglects random thermal motion of the ions and electrons.

The ion beam between the ion emitter and the neutralization grid is determined, as is the mixed ion-electron beam downstream of the neutralization grid. The ion-electron beam is found to have a small-wavelength, small-amplitude periodic wave structure. A similar ion-electron-beam wave structure may exist upstream of the neutralization grid if this grid is relatively far downstream of the accelerating grid.

The forces on the individual grids and the overall thrust and specific impulse of the ion rocket are found using momentum-integral concepts, which are discussed in an appendix. It is shown that the ion-emitting grid can experience only a drag force, the accelerating grid can experience a drag or a thrust force, and the neutralizing grid can experience only a thrust force.

The analysis also indicates that the spacing between the acceleration and neutralization grids does not affect the thrust and specific impulse of the ion rocket. In particular, when the spacing between these grids is relatively large, electrons move upstream from the neutralizing grid and eliminate the tendency toward ion current reversal or excessive beam spreading that would otherwise occur.

INTRODUCTION

Considerable interest exists in the utilization of ion rockets as low-thrust, high-specific-impulse propulsion units for space flight. References 1 to 9 are recent examples of mission studies (refs. 1 to 3) and of ion-rocket design and performance studies (refs. 4 to 9).

The current NASA Lewis Research Center program relating to ion-rocket design and testing is outlined in reference 4. As part of that program, theoretical one-dimensional analyses have been made concerning the acceleration and mixing of ion and electron beams. The results of these one-dimensional analyses are presented herein and in the concurrent investigation reported in reference 10.

Reference 10 considers the effect of thermal motion on ion and electron acceleration and deceleration, the neutralization of an ion beam by mixing with an electron beam, and the electrical breakdown and manufacturing tolerance limitations on accelerator design. The advantages of using an "accelerate-decelerate" design principle in ion and electron accelerators are also discussed (see also refs. 4, 8, and 9). Reference 10 does not treat a specific ion-rocket configuration, but rather considers the performance of various types and arrangements of ion and electron accelerators that may be incorporated in an ion-rocket design.

In the present report attention is focused on a specific one-dimensional configuration that employs the accelerate-decelerate principle and consists of an ion-emitting grid, an accelerating grid, and a decelerating-neutralizing grid. Details of the resulting ion-beam and electron-ion-beam flows are discussed. The object is to give a detailed, integrated discussion of a basic ion-rocket configuration.

The application of the momentum-integral method for computing ion-rocket thrust is discussed in an appendix and is employed in the body of the report to determine overall ion-rocket thrust and the forces on the individual grids. A general discussion of the behavior of one-dimensional ion or electron beams is given in other appendixes.

The one-dimensional beam solutions presented herein neglect random thermal motion. That is, it is assumed that all the ions or electrons at a given station have the same velocity. For a mixed electron-ion beam the local electron velocity differs (in general) from the local ion velocity. In the case of an electron or ion beam with current reversal, the upstream and downstream moving particles have the same local speed.

ANALYSIS

The one-dimensional configuration studied herein is indicated in figure 1(a). The corresponding voltage variation V is given in figure 1(b). (Symbols are defined in appendix A.) Ions are assumed to be emitted with essentially zero velocity by a grid at x_e. The ion-emitting grid is considered to be at zero voltage so that the local ion velocity at any station is proportional to $\sqrt{-V}$ (appendix B).

The ions emitted at x_e are accelerated (to a value above the desired final value) by an accelerating grid at $x = 0$. A grid at $x = x_n$ both decelerates the ions (to the desired final velocity) and neutralizes them (by emitting electrons in a one-to-one correspondence with the oncoming positive charges). Despite the dual role of the latter grid (i.e., deceleration and neutralization of the ions), it will be referred to as the neutralization grid. Downstream of x_n there is a mixed ion and electron beam (fig. 1(a)) having small-amplitude, small-wavelength cyclic variations of V with x (as will be derived). It is initially assumed that the neutralizing grid is sufficiently close to the accelerating grid that V increases monotonically from $x = 0$ to $x = x_n$ as indicated in figure 1(b). The resulting electric field prevents electrons from moving upstream of the neutralizing grid.

In the following sections, details of the ion beam in the acceleration ($x_e \leq x < 0$) and deceleration ($0 < x < x_n$) regions are presented assuming that the random thermal motion of the ions is negligible. The mixed ion-electron beam downstream of the neutralizing grid is then analyzed. Next, expressions for the forces on the grids and the overall thrust and specific impulses are found. Finally, an analysis is presented for the case wherein the neutralizing grid is relatively far downstream of the accelerating grid, resulting in electrons being present between these grids.

The mks system of measurement is used throughout. Subscripts + and - are used only when it is necessary to distinguish between ion and electron properties, respectively.

Ion Flow in Acceleration and Deceleration Regions

The equations of motion for a one-dimensional ion beam are integrated in appendixes B and C, neglecting random thermal motion. In appendix B it is assumed that the ion current is in the +x direction only, while in appendix C two-way ion currents are considered. These solutions were previously derived in reference 11 in connection with electron vacuum-tube performance and are summarized in other sources (such as ref. 12). In the present section the results of appendix B (i.e., one-way currents) are applied to discuss the flow in the acceleration and deceleration regions of the ion rocket of figure 1.

Appendix B utilizes the following nondimensional variables for V and x, respectively:

$$\varphi = \frac{V}{V_0} \tag{B5a}$$

$$\xi = \frac{x}{L}\sqrt{\frac{j}{j_M}} \tag{B5b}$$

where

$$j_M \equiv -\frac{4}{9}\epsilon_0\sqrt{-2\eta V_0}\,\frac{V_0}{L^2} \tag{B6}$$

Here V_0 is the voltage at $x = 0$, L is the spacing between the emitter and accelerator grids, and j_M is the maximum (space-charge-limited) current, which results from an electrode spacing L and voltage difference V_0. Equation (B6), which is sometimes referred to as Child's law (ref. 13), gives the maximum current that can pass through the ion rocket (for given V_0, L). Note that $\varphi = 1$ and $\xi = 0$ at the accelerator grid.

Integral curves of φ against ξ, from appendix B, are presented in figure 2 for $\varphi \geq 0$. Two types of integral curves, referred to as type C and type D, are noted. Type C integral curves are characterized by the fact that there is a point (ξ^*, φ^*) on each of these curves at which $\varphi' = 0$. Type D curves do not have this critical point. The parameters φ^* and β are used to identify particular type C and D curves, respectively (see eqs. (B10) for relation between φ^*, β, and φ_0'). In figure 2, curve a is the envelope of the right-hand branches of the type C curves, curve b is the right-hand branch of the $\varphi^* = 0$ integral curve, and curve d is the locus of the minimum points on the type C curves. Expressions for these curves are given by equations (B12), (B14), and (B15). The type C and D integral curves for $\xi < 0$ are the mirror image of those for $\xi > 0$. Further details are given in appendix B.

The ion flow in the accelerating and decelerating regions of the ion rocket can be discussed in terms of the type C and type D integral curves of appendix B. This discussion follows.

Acceleration region $\xi_e \leq \xi < 0$. - The value of ξ at the ion-emitting grid is

$$\xi_e = \frac{x_e}{L}\sqrt{\frac{j}{j_M}} = -\sqrt{\frac{j}{j_M}} \tag{1}$$

Since $0 < j/j_M \leq 1$, then $-1 \leq \xi_e < 0$. The voltage and velocity are assumed zero at this station so that

$$\varphi_e = v_e = 0 \tag{2}$$

All the type D integral curves and also the type C integral curve for $\varphi^* = 0$ are possible solutions for the accelerator region (see sketch (a)).

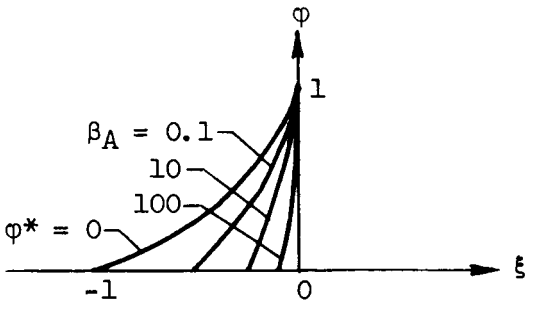

(a)

For $\xi_e = -1$ (i.e., $j = j_M$), the ion flow is defined by (from eq. (B11) with $\varphi^* = 0$)

$$\varphi = (1 + \xi)^{4/3} \tag{3}$$

which is Child's result (ref. 13). Note that φ', and therefore the electric field, is zero at $\xi = -1$, which confirms that equation (3) corresponds to space-charge-limited current flow.

For $-1 < \xi_e < 0$ (i.e., $0 < j/j_M < 1$), the variation of φ with ξ is (from eq. (B16))

$$\xi = (\sqrt{\varphi} - 2\sqrt{\beta_A})\sqrt{\sqrt{\varphi} + \sqrt{\beta_A}} - (1 - 2\sqrt{\beta_A})\sqrt{1 + \sqrt{\beta_A}} \tag{4}$$

The subscript A is used for β to distinguish type D integral curves in the acceleration region from type D integral curves in the deceleration region. The relation between ξ_e and β_A is (letting $\xi = \xi_e$ and $\varphi = 0$ in eq. (4))

$$\xi_e = -2\beta_A^{3/4} - (1 - 2\sqrt{\beta_A})\sqrt{1 + \sqrt{\beta_A}} \tag{5}$$

Equations (4) and (5) apply when the ion emitter is emission-limited. Note that equation (4) reduces to equation (3) for $\beta_A = 0$.

Deceleration region $0 < \xi < \xi_n$. - The integral curve describing the ion flow in the deceleration region depends on the voltage and location of the neutralizing grid. For the present, it is assumed that

$$0 < \xi_n < \xi_d(\varphi_n) \tag{6}$$

where

$$\xi_d(\varphi) = (1 + 2\sqrt{\varphi})\sqrt{1 - \sqrt{\varphi}} \tag{7}$$

is the equation of curve d in figure 2 (see eq. (B15)). That is, the neutralizing grid is assumed to be sufficiently close to the accelerating grid so that ξ_n is upstream of curve d (as indicated in sketch (b)). Under these conditions, φ decreases monotonically from $\varphi = 1$ at $\xi = 0$ to $\varphi = \varphi_n$ at $\xi = \xi_n$. The resulting electric field prevents electrons from moving upstream of the neutralizing grid. The beam in

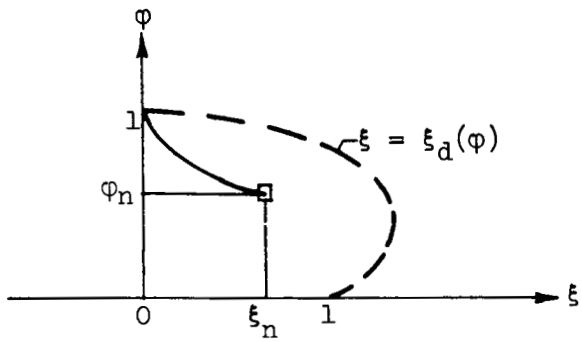

(b)

the deceleration region contains only ions, and the type C and D integral curves apply. The case where ξ_n is greater than $\xi_d(\varphi_n)$ is discussed in the section preceding CONCLUDING REMARKS.

The variation of ξ with φ for type C flows is (from eqs. (B11))

$$\xi - \xi^* = (\sqrt{\varphi} + 2\sqrt{\varphi^*})\sqrt{\sqrt{\varphi} - \sqrt{\varphi^*}} \tag{8}$$

where

$$\xi^* = (1 + 2\sqrt{\varphi^*})\sqrt{1 - \sqrt{\varphi^*}}$$

For type D flows (from eq. (B16))

$$\xi = -(\sqrt{\varphi} - 2\sqrt{\beta_D})\sqrt{\sqrt{\varphi} + \sqrt{\beta_D}} + (1 - 2\sqrt{\beta_D})\sqrt{1 + \sqrt{\beta_D}} \tag{9}$$

The integral curve corresponding to a given (ξ_n, φ_n) is found by substituting (ξ_n, φ_n) into equation (8) or (9) and solving for φ^* or β_D.

Flow Downstream of Neutralizing Grid

The neutralizing grid emits electrons in a one-to-one correspondence with the oncoming positive charges. As a result there is a mixed electron-ion beam downstream of ξ_n (fig. 1). This mixed beam is now analyzed assuming that the electrons are emitted with essentially zero

velocity and that the electron current is space-charge-limited at ξ_n. It is further assumed that no electron-ion recombination occurs. Subscripts + and - are used to differentiate ion and electron properties, respectively. Quantities such as ρ_q and $\eta = \rho_q/\rho_m$ are positive or negative for ions or electrons, respectively. Similarly, current density $j = \rho_q v$ is a signed quantity, the sign depending on the sign of ρ_q and v.

Downstream of the neutralization grid the ion current j_+ equals the negative of the electron current j_- (assuming steady state), so that

$$j_+ \equiv (\rho_q v)_+ = -j_- \equiv -(\rho_q v)_- \tag{10}$$

The velocity of the ions is (eqs. (B3) and (B5a))

$$v_+ = \sqrt{-2\eta_+ V_0 \varphi} \tag{11a}$$

Similarly, the velocity of the electrons is (assuming $v_- = 0$ at $\varphi = \varphi_n$)

$$v_- = \sqrt{-2\eta_- V_0 (\varphi - \varphi_n)} \tag{11b}$$

Poisson's equation can then be written as

$$\frac{d^2\varphi}{dx^2} = -\frac{\left(\rho_{q_+}\right) + \left(\rho_{q_-}\right)}{\epsilon_0 V_0}$$

$$= \frac{j_+}{\epsilon_0 V_0^{3/2}\sqrt{-2\eta_+\varphi_n}}\left(\sqrt{\frac{\delta\varphi_n}{\varphi_n - \varphi}} - \sqrt{\frac{\varphi_n}{\varphi}}\right) \tag{12}$$

where

$$\delta \equiv \frac{\eta_+}{-\eta_-} \doteq \frac{1}{1835}\,\frac{z}{\text{A.W.}} \ll 1 \tag{13}$$

The symbol z represents the number of charges per ion (which can be taken to be 1), and A. W. is the atomic weight of the ion. For $x = 1$, δ represents the ratio of the mass of an electron to that of an ion. In general, δ is very small.

Equation (12) is to be solved for φ subject to the boundary conditions

$$\varphi(\xi_n) = \varphi_n \tag{14a}$$

$$\varphi'(\xi_n) = 0 \tag{14b}$$

where equation (14b) corresponds to space-charge-limited electron emission from the neutralizing grid. If recombination of ions and electrons is considered negligible, j_+ is constant in equation (12) and may be taken to equal the ion current in the acceleration and deceleration sections of the ion rocket. The neglect of recombination is later shown to be valid.

From physical reasoning it is expected that the electron velocity in the beam will be of the same order of magnitude as the ion velocity at ξ_n, so that (from eq. (11))

$$\frac{\varphi_n - \varphi}{\varphi_n} = O(\delta) \tag{15}$$

For δ small, φ departs only slightly from φ_n and a perturbation method of solution is possible. Let

$$\frac{\varphi}{\varphi_n} = 1 - \delta\Phi + O(\delta^2) \tag{16}$$

Introduce the new independent variable

$$\zeta = \frac{2}{3}\sqrt{\left(\frac{j}{j_M}\right)_+}\left(\frac{1}{\varphi_n}\right)^{3/4}\frac{1}{\sqrt{\delta}}\left(\frac{x - x_n}{L}\right) \tag{17}$$

Substituting equations (16) and (17) into equation (12) and neglecting terms of order δ compared with 1 yield

$$\frac{d^2\Phi}{d\zeta^2} = \frac{1}{\sqrt{\Phi}} - 1 \tag{18a}$$

with the boundary conditions (from eq. (14))

$$(\Phi)_{\zeta=0} = (d\Phi/d\zeta)_{\zeta=0} = 0 \tag{18b}$$

Integration of equations (18) yields

$$\frac{d\Phi}{d\zeta} = \pm\sqrt{2\sqrt{\Phi}(2 - \sqrt{\Phi})} \tag{19}$$

Consideration of equations (18a) and (19) shows that the curve of Φ against ζ is cyclic having a minimum point at $\Phi = 0$ and a maximum point at $\Phi = 4$. Integrating equation (19) shows that, for the first half cycle,

$$\zeta = 2\sqrt{2}\,\sin^{-1}\sqrt{\frac{\sqrt{\Phi}}{2}} - \sqrt{2\sqrt{\Phi}(2 - \sqrt{\Phi})} \qquad \begin{cases} 0 \le \zeta \le \sqrt{2}\,\pi \\ 0 \le \Phi \le 4 \end{cases} \tag{20}$$

The variation of ζ with Φ, for the remaining cycles, is found by symmetry. The curve of Φ against ζ is indicated in sketch (c).

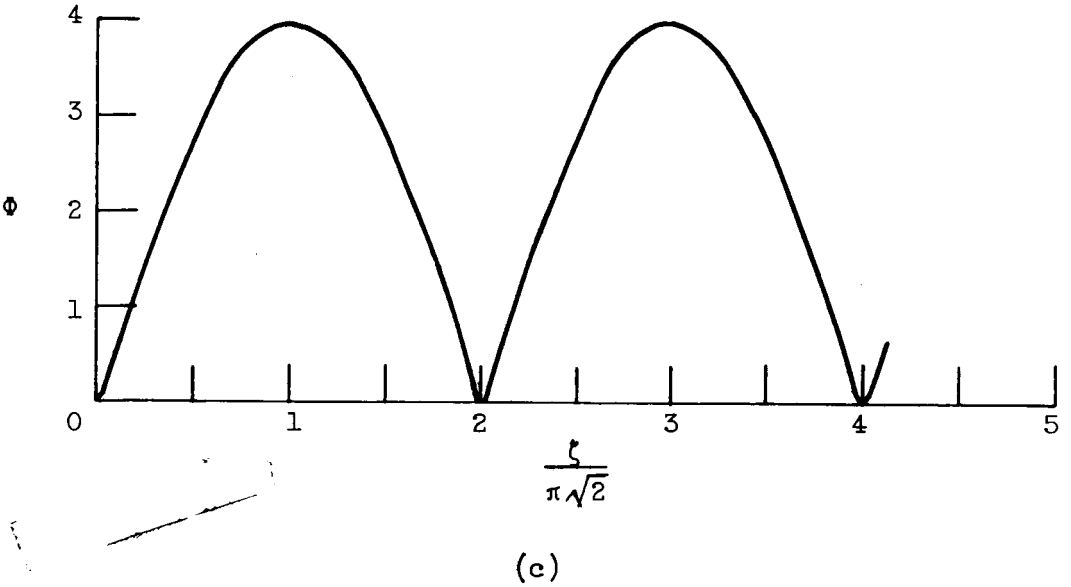

(c)

Thus, there is a standing wave in the ion-electron beam with a wavelength

$$\Delta\zeta = 2\sqrt{2}\,\pi$$

which corresponds to the physical distance $\Delta x = \lambda$ given by

$$\frac{\lambda}{L} = 3\sqrt{2}\,\pi\,\varphi_n^{3/4}\sqrt{\left(\frac{j_M}{j}\right)_+}\sqrt{\delta} \tag{21}$$

Unless $(j_M/j)_+ \gg 1$, the wavelength λ is small compared with L. For current designs, L is of the order of 1 centimeter (ref. 4). Thus, the assumption of no recombination appears to be valid, at least for several periodic variations of the potential (see also ref. 10).

To the present approximation, the ion velocity, referenced to the ion velocity at ξ_n, is (eqs. (11a) and (16))

$$\frac{v_+}{(v_+)_n} = \sqrt{\frac{\varphi}{\varphi_n}} = 1 - \frac{\delta}{2}\Phi + O(\delta^2) \tag{22}$$

Thus, the ions move with essentially the constant velocity $(v_+)_n$. Periodic decreases of ion velocity, from the $(v_+)_n$ value, are of order δ. The electron velocity, referenced to $(v_+)_n$, is (eqs. (11), (13), and (16))

$$\frac{v_-}{(v_+)_n} = \sqrt{\frac{\varphi_n - \varphi}{\delta\varphi_n}} = \sqrt{\Phi}\left[1 + O(\delta)\right] \tag{23}$$

Since $\sqrt{\Phi}$ varies from 0 to 2, the electron velocity varies periodically from a value of zero to a value equal to twice $(v_+)_n$. The electric field, referenced to $-V_0/L$ (which is a measure of the electric field in the accelerator) is (from eqs. (16), (17), (19), and (B2))

$$\frac{E}{-V_0/L} = \pm\frac{2}{3}\sqrt{\left(\frac{j}{j_M}\right)_+}\varphi_n^{1/4}\sqrt{2\sqrt{\Phi}(2-\sqrt{\Phi})}\sqrt{\delta}\left[1 + O(\delta)\right] \tag{24}$$

for $d\Phi/d\zeta \lesseqgtr 0$. The electric field, as expressed in equation (24), is of order $\sqrt{\delta}$ and is relatively small compared with the electric field in the accelerator.

Reference 10 considers the case of neutralization by the mixing of electron and ion beams. It was found that the maximum velocity which the electrons can have, without partial current reversal, is twice the ion velocity. The corresponding solution for the mixed ion-electron beam, obtained previously in reference 10, is similar to that presented herein, although the initial conditions and the derivations are somewhat different. Reference 10 points out that the wavelength (of the standing wave in the ion-electron beam) equals the ion velocity $(v_+)_n$ divided by the electron plasma frequency, $\frac{1}{2\pi}\sqrt{\frac{1}{\delta}\frac{\left[\eta(\rho_q)_n\right]_+}{\epsilon_0}}$.

Thrust, Specific Impulse, and Power Considerations

The application of the momentum-integral method for evaluating ion-rocket thrust is discussed in appendix D. The results of that appendix are now used to determine the overall thrust and the forces on the ion-rocket grids. In addition, specific impulse and electrical power requirements are noted.

The net reactive force per unit cross-sectional area f, developed between any two stations x_α and x_β in a one-dimensional charged beam, is (eq. (D8))

$$f = \left[\frac{\epsilon_0 E^2}{2} - \rho_m v^2\right]_{x_\alpha}^{x_\beta} \tag{25a}$$

$$= \left[\frac{\epsilon_0 E^2}{2} - \frac{jv}{\eta}\right]_{x_\alpha}^{x_\beta} \tag{25b}$$

where $x_\beta > x_\alpha$. A positive value of f indicates that the force due to the beam is in the +x (i.e., drag) direction. The net thrust of an ion rocket can be found by taking x_α to be upstream of the ion emitter (its contribution to thrust is then zero) and taking x_β to be downstream of the neutralizing grid. The simplest procedure is to take x_β to be on the downstream side of the neutralizing grid so that $E = v_- = 0$ (by assumption, for the present model) and $v_+ = (v_+)_n = \sqrt{-2\eta_+ V_0 \varphi_n}$. Equation (25b) then gives (using eq. (B5a))

$$\frac{f}{\frac{8}{9}\epsilon_0\left(\frac{j}{j_M}\right)_+\left(\frac{V_0}{L}\right)^2} = -\sqrt{\varphi_n} \tag{26}$$

as the net thrust of the ion rocket. The negative sign indicates that the force is in the -x (thrust) direction. The same result would be obtained regardless of where x_β was taken, provided it is downstream of x_n. The specific impulse (thrust divided by the net weight-flow rate in the neutralized beam) is (in seconds)

$$I_s = \frac{\sqrt{-2\eta_+ V_0 \varphi_n}}{(1+\delta)g} \tag{27}$$

where g is the gravitational acceleration constant (9.807 m/sec^2). The term $1 + \delta$ appears so as to include the weight of the electrons in the neutralized beam and is negligible in most cases.

Equations (26) and (27) indicate $f \sim \left(\frac{j}{j_M}\right)_+ \sqrt{V_n} V_0^{3/2}$ and $I_s \sim \sqrt{|V_n|}$. For a given mission, there is usually an optimum value of I_s resulting in minimum propellant and powerplant weight. This fixes V_n. The value of f can be increased (for a given geometry and a given V_n) by increasing V_0. The ability to vary thrust and specific impulse of a given configuration independently is one of the major advantages of the accelerate-decelerate cycle (refs. 4, 8, 9, and 10). Another advantage is that the electric field in the deceleration region prevents electrons from entering the ion accelerator and interfering with ion emission and acceleration therein.

The force on each individual grid is most easily found by taking x_α and x_β to be infinitesimal distances upstream and downstream of the grid, respectively (appendix D). Assuming there are neither flow nor electrical forces upstream of x_e, the force on the emitter grid is (from eqs. (D12) and (B17a))

$$\frac{(f)_{x_e}}{\frac{8}{9}\epsilon_0\left(\frac{j}{j_M}\right)_+\left(\frac{V_0}{L}\right)^2} = \sqrt{\beta_A} \tag{28}$$

where $\beta_A > 0$ corresponds to type D flows (emission-limited) in the accelerator, and $\beta_A = 0$ corresponds to a Child's law ($\varphi^* = 0$, space-charge-limited) acceleration. The force on the accelerating grid is (from eqs. (D12) and (B17a))

$$\frac{f_0}{\frac{8}{9}\epsilon_0\left(\frac{j}{j_M}\right)_+\left(\frac{V_0}{L}\right)^2} = -\sqrt{\varphi^*} - \sqrt{\beta_A} \qquad \text{Type C} \qquad (29a)$$

$$= \sqrt{\beta_D} - \sqrt{\beta_A} \qquad \text{Type D} \qquad (29b)$$

Here types C and D refer to the integral curve in the deceleration region. The force on the neutralizing grid is (assuming $E = v_- = 0$ on the downstream side)

$$\frac{(f)_{x_n}}{\frac{8}{9}\epsilon_0\left(\frac{j}{j_M}\right)_+\left(\frac{V_0}{L}\right)^2} = -\sqrt{\varphi_n} + \sqrt{\varphi^*} \qquad \text{Type C} \qquad (30a)$$

$$= -\sqrt{\varphi_n} - \sqrt{\beta_D} \qquad \text{Type D} \qquad (30b)$$

where types C and D again refer to the integral curve in the deceleration region. The net force on the three grids agrees with equation (26), as expected.

Equations (28) to (30) may be of interest for structural design. It is interesting to note that some of the grids can experience drag rather than thrust. In particular, the ion emitter can experience only a drag force, while the accelerating grid can experience a drag force if equation (29b) applies and $\beta_D > \beta_A$. The neutralizing grid will always experience a thrust force.

Impingement of ions on the accelerator and neutralizing grids will result in reduced thrust and specific impulse. The performance of an ion rocket, with ion impingement, can be readily evaluated. Let Y_0 be the fraction of the emitted ions that strike the accelerator grid, and let Y_n be the fraction of the emitted ions that strike the neutralizing grid. For a given φ_n, the actual thrust and specific impulse, referenced to the "no impingement" values, are then

$$\frac{f_{ac}}{f} = \frac{(I_s)_{ac}}{I_s} = 1 - Y_0 - Y_n \qquad (31)$$

Ideally, the only electrical power required in the configuration of figure 1 is that required to "pump" electrons from the voltage at x_e to the voltage at x_n. This power per unit area of the beam equals

$$P = j_- V_n = j_+ |V_n| \tag{32a}$$

Thus, there is no cost in electrical power associated with the over-acceleration of the ions. However, if some ions impinge on the accelerating grid, a corresponding electron current to this grid will be required to maintain steady-state conditions. The net power required (compared with the no-impingement value) is then

$$\frac{P_{ac}}{P} = 1 + Y_0\left(\frac{1}{\varphi_n} - 1\right) \tag{32b}$$

Thus, small values of φ_n (i.e., large overaccelerations) can result in large additional power requirements unless Y_0 is kept small.

Effect of Neutralizing-Grid Location Downstream of Curve d

Up till now it has been assumed that the neutralizing grid is upstream of curve d so that φ decreases monotonically from the value 1, at $\xi = 0$, to the value φ_n, at $\xi = \xi_n$ (sketch (b)). The resulting electric field prevents electrons from moving upstream of the neutralizing grid. In the present section, the effect of locating the neutralization grid downstream of curve d is considered. Appendixes B and C and figures 2 to 4 indicate that the integral curve will then have a minimum point upstream of ξ_n if electrons are not present. If the neutralizing grid emits electrons, these will be attracted toward the potential minimum, and the integral curve between $\xi = 0$ and $\xi = \xi_n$ will be modified. A particular solution for this modified integral curve is presented herein, neglecting thermal motions of the ions and electrons.

Consider a neutralizing-grid location and potential as indicated in figure 5. If no electrons are emitted at ξ_n, the integral curve for $0 < \xi < \xi_n$ will be a type C integral curve as indicated in figure 5(a). However, if electrons are emitted at ξ_n, the integral curve will be modified. A possible solution for the resulting integral curve is indicated in figure 5(b). The ions follow the type C curve $\varphi^* = \varphi_n$ from $\xi = 0$ to $\xi = \xi_d(\varphi_n)$. From $\xi_d(\varphi_n)$ to ξ_n there is a mixed ion-electron beam whose potential departs only slightly from φ_n. The flow in this region, $\xi_d(\varphi_n) < \xi < \xi_n$, is found as follows.

The neutralizing grid emits a downstream electron current $(j_-)_D$, and an upstream electron current $(j_-)_U$, as indicated in figure 5(c). Note $(j_-)_D$ is negative while $(j_-)_U$ is positive. The upstream current $(j_-)_U$ is reflected at $\xi_d(\varphi_n)$ and then proceeds downstream as the electron current $-(j_-)_U$. For steady-state conditions, the electron and ion currents, downstream of ξ_n, are equal and opposite so that

$$-(j_+) = (j_-)_D + \left[-(j_-)_U\right] \tag{33a}$$

or

$$\frac{j_+}{(j_-)_U} = 1 + \frac{(j_-)_D}{-(j_-)_U} \tag{33b}$$

The electrons are assumed to be emitted with zero velocity, so that the ion and electron velocities are, respectively,

$$v_+ = \sqrt{-2\eta_+ V_0 \varphi}$$

$$v_- = \pm\sqrt{-2\eta_- V_0 (\varphi - \varphi_n)}$$

The local charge density is then

$$\rho_{q+} = \frac{j_+}{\sqrt{-2\eta_+ V_0 \varphi}} \tag{34a}$$

$$\rho_{q-} = \frac{-2(j_-)_U}{\sqrt{-2\eta_- V_0 (\varphi - \varphi_n)}} \tag{34b}$$

where equation (34b) applies only for $\xi_d(\varphi_n) < \xi < \xi_n$. Poisson's equation for this region is

$$\frac{d^2\varphi}{dx^2} = -\frac{\rho_{q+} + \rho_{q-}}{\epsilon_0 V_0}$$

$$= \frac{j_+}{\epsilon_0 V_0 \sqrt{-2\eta_+ V_0 \varphi_n}} \left(\alpha \sqrt{\frac{\delta\varphi_n}{\varphi - \varphi_n}} - \sqrt{\frac{\varphi_n}{\varphi}} \right) \tag{35}$$

where

$$\alpha \equiv \frac{2(j_-)_U}{j_+} \equiv \frac{2}{1 + \dfrac{(j_-)_D}{-(j_-)_U}} \tag{36a}$$

The parameter α lies between the limits

$$0 \leq \alpha \leq 2 \tag{36b}$$

which correspond to the limiting values $-(j_-)_U = 0$ and $(j_-)_D = 0$. Equation (35) can be written (introducing Φ and ζ as defined by equations (16) and (17) and neglecting higher-order terms)

$$\frac{d^2\Phi}{d\zeta^2} = \frac{\alpha}{\sqrt{\Phi}} - 1 \tag{37}$$

The boundary conditions at $\zeta = 0$ are again taken to be

$$(\Phi)_{\zeta=0} = \left(\frac{d\Phi}{d\zeta}\right)_{\zeta=0} = 0 \tag{38}$$

The boundary condition $(\Phi)_{\zeta=0} = 0$ follows from the definition of Φ, and the boundary condition $(d\Phi/d\zeta)_{\zeta=0}$ assumes that the electron emission in the upstream direction is space-charge-limited.

Integration of equation (37), with the boundary conditions of equation (38), gives

$$\frac{d\Phi}{d\zeta} = \pm\sqrt{2\sqrt{\Phi}(2\alpha - \sqrt{\Phi})} \tag{39}$$

where Φ is periodic and varies between the limits

$$0 \leq \Phi \leq 4\alpha^2 \tag{40}$$

Let ζ_0 be a value of ζ for which $\Phi = 0$. The variation of Φ with ζ is (for half a cycle)

$$\zeta - \zeta_0 = 2\sqrt{2}\,\alpha \sin^{-1}\sqrt{\frac{\sqrt{\Phi}}{2\alpha}} - \sqrt{2\sqrt{\Phi}(2\alpha - \sqrt{\Phi})} \qquad \begin{cases} 0 \leq \zeta - \zeta_0 \leq \sqrt{2}\,\pi\alpha \\ 0 \leq \Phi \leq 4\alpha^2 \end{cases} \tag{41}$$

The remainder of the integral curve is found by symmetry. The wavelength is

$$\Delta\zeta = 2\sqrt{2}\,\pi\alpha$$

which corresponds to the physical distance $\Delta x \equiv \lambda$ given by

$$\frac{\lambda}{L\sqrt{\left(\frac{j_M}{j}\right)_+}} = 3\sqrt{2}\,\pi\,\alpha\,\varphi_n^{3/4}\sqrt{\delta} \tag{42}$$

Comparison with equation (21) shows that the wavelength is α times that of the ion-electron beam downstream of ξ_n.

Since the potential and electric field must be continuous at $\xi_d(\varphi_n)$, and since the ions were assumed to follow a $\varphi^* = \varphi_n$ integral

curve, it follows that $\Phi = d\Phi/d\zeta = 0$ at $\xi_d(\varphi_n)$. Hence, there must be an integral number of cycles (denoted by the integer N) between $\xi_d(\varphi_n)$ and ξ_n, or

$$\frac{N\lambda}{L\sqrt{\left(\frac{j_M}{j}\right)_+}} = \xi_n - \xi_d(\varphi_n) \tag{43}$$

Substituting equation (42) into (43) and solving for α give

$$\alpha = \frac{\xi_n - \xi_d(\varphi_n)}{3\sqrt{2}\ \pi\ \varphi_n^{3/4}\sqrt{\delta}}\ \frac{1}{N} \tag{44}$$

Equation (44) gives the discrete values of α, corresponding to integral values of N, which satisfy the boundary conditions $\Phi = d\Phi/d\zeta = 0$ at $\xi = \xi_d(\varphi_n)$ and ξ_n.

For $\alpha = 2$ (i.e., $(j_-)_D = 0$), all the electron current from the neutralizing grid first moves upstream, is reflected at $\xi_d(\varphi_n)$, and then goes downstream. The flow in the region $\xi_d(\varphi_n) < \xi < \xi_n$ is periodic and has a wavelength λ and perturbation amplitude $\sqrt{\Phi}$ that are twice those for $\xi > \xi_n$. Substitution of $\alpha = 2$ into equation (44) defines the smallest possible value of N for a given configuration. When $\alpha = 1$ (i.e., $(j_-)_D = -(j_-)_U$), the wavelength and perturbation amplitude are the same as those for $\xi > \xi_n$. If the electron emission at ξ_n is from circular wires, it would seem that α should be approximately 1. In the limit as $\alpha \to 0$ (i.e., $(j_-)_U \to 0$), the wavelength and perturbation amplitude both tend to zero. However, regardless of how small α is (so long as it is not zero), a periodic solution of the type indicated in figure 5 will result (neglecting random thermal motions).

The solution indicated in figure 5(b) is applicable regardless of how far ξ_n is downstream of curve d. This modification of the type C or type B integral curves (which would otherwise occur in $0 < \xi < \xi_n$) is beneficial in that it probably will reduce excessive ion-beam spreading or ion current reversal. However, the presence of electrons upstream of ξ_n makes the flow more complex and may make theoretical three-dimensional designs (designed to avoid excessive ion impingement on the neutralizing grid) more difficult. For ion rockets employing the integral curve noted in figure 5(b), the net thrust is still given by equation (26). All the thrust is exerted on the accelerating grid. (The ion-emitting and neutralizing grids experience no force.)

CONCLUDING REMARKS

The one-dimensional analysis indicates that the spacing between the acceleration and neutralization grids does not affect the thrust and specific impulse of an ion rocket. In particular, when the spacing between these grids is relatively large, electrons move upstream from the neutralizing grid and eliminate the tendency toward ion current reversal or excessive ion-beam spreading that would otherwise occur.

Lewis Research Center
National Aeronautics and Space Administration
Cleveland, Ohio, December 9, 1959

APPENDIX A

SYMBOLS

Units are mks throughout the report.

B_i	magnetic induction
D_i	electric displacement
E, E_i	electric-field strength
F_i	net force exerted on body
f	force per unit area exerted on one-dimensional grids
H_i	magnetic field
I_s	specific impulse
j	current density, $\rho_q v$ (signed)
j_e, j_r, j_t	emitted, reflected, and transmitted currents (appendix C)
j_M	space-charge-limited current density, eq. (B6)
j_{tot}	sum of magnitudes of upstream and downstream currents
$(j_-)_U$, $(j_-)_D$	upstream and downstream electron currents, respectively, emitted by neutralization grid
L	distance between ion emitter and acceleration grid
N	integer
P	electrical power consumption per unit beam area, eq. (32)
T_{ij}	Maxwell stress tensor, eq. (D2)
V	voltage relative to ion emitter
V_0	voltage of acceleration grid
v	velocity, positive in +x direction
X_i	body force

x	streamwise distance
x_i	Cartesian coordinates
x_α, x_β	upstream and downstream stations, respectively
Y_0, Y_n	fraction of emitted ions impinging on acceleration and neutralization grids, respectively
Z	j_t/j_e
α	current ratio, eq. (36a)
β	parameter characterizing type D integral curves, eq. (B10b)
β_A, β_D	values of β in acceleration and deceleration regions, respectively
δ	perturbation parameter, eq. (13)
ϵ_0	dielectric constant for a vacuum, 8.854×10^{-12} farad/m
ζ	nondimensional variable for streamwise distance, eq. (17)
η	charge-to-mass ratio of an electron or ion, ρ_q/ρ_m (signed)
λ	wavelength in units of x
ξ	nondimensional streamwise distance, $\frac{x}{L}\sqrt{\frac{j}{j_M}}$
ξ^*	value of ξ at minimum point of type C curve
ρ_m	mass density, per unit volume
ρ_q	charge density, per unit volume (signed)
Φ	nondimensional voltage perturbation, eq. (16)
φ	nondimensional voltage, V/V_0
φ^*	value of φ at minimum point of type C curve

Subscripts:

a	associated with curve a, eq. (B12)
ac	actual

b — associated with curve b, eq. (B14)

d — associated with curve d, eq. (B15)

e — associated with ion emitter (at x_e)

i, or j — vector components 1, 2, and 3

ij — tensor

n — associated with neutralizing grid (at x_n)

0 — associated with accelerating grid (at $x = 0$)

+,- — properties associated with ions and electrons, respectively

Superscript:

' — denotes differentiation with respect to ξ

APPENDIX B

ONE-DIMENSIONAL CHARGED BEAM WITHOUT CURRENT REVERSAL

The equations of motion for a one-dimensional, single-species charged beam are integrated herein assuming all the charges move in the +x direction and neglecting random thermal motions. Flows with current reversal are considered in appendix C. The solutions apply equally for positively or negatively charged beams, and the subscripts + and - are therefore omitted. These solutions have been previously obtained in reference 11 (see also, ref. 12) and are rederived here to facilitate discussion. They are applied in the body of the report to describe the ion beam in the acceleration and deceleration portions of an ion rocket.

The equations of motion for a one-dimensional charged beam are

$$\text{Conservation of charge:} \quad \rho_q v = j \tag{B1a}$$

$$\text{Poisson's equation:} \quad \frac{dE}{dx} = \frac{\rho_q}{\epsilon_0} \tag{B1b}$$

$$\text{Momentum equation:} \quad \rho_m v \frac{dv}{dx} = \rho_q E \tag{B1c}$$

The voltage is related to the electric field by

$$E = -\frac{dV}{dx} \tag{B2}$$

Since $(\rho_q/\rho_m) \equiv \eta$ is a constant, equation (B1c) can be integrated to yield (defining V to be zero when $v = 0$)

$$v = \sqrt{-2\eta V} \tag{B3}$$

For positive ions, η is positive and V is negative (or zero). Combining equations (B1a), (B1b), (B2), and (B3) yields

$$\frac{d^2V}{dx^2} = \frac{-j}{\epsilon_0\sqrt{-2\eta V}} \tag{B4}$$

which can be integrated to find the variation of V with x. It is convenient first to nondimensionalize the dependent and independent variables with respect to conditions at $x = 0$. Thus, replace (V,x) by the variables (φ,ξ) defined according to

$$\varphi = \frac{V}{V_0} \tag{B5a}$$

$$\xi = \frac{x}{L}\sqrt{\frac{j}{j_M}} \tag{B5b}$$

where

$$j_M \equiv -\frac{4}{9}\epsilon_0\sqrt{-2\eta V_0}\,\frac{V_0}{L^2} \tag{B6}$$

The quantity j_M is the maximum current (i.e., the space-charge-limited current) that can be obtained with an emitter-accelerator spacing L and a voltage difference V_0. Equation (B6) is often referred to as Child's law (ref. 13). Equation (B4) can then be written

$$\varphi'' = \frac{4}{9}\frac{1}{\sqrt{\varphi}} \tag{B7}$$

where the prime indicates differentiation with respect to ξ. The boundary conditions may be taken to be

$$\varphi(0) = 1 \tag{B8a}$$

$$\varphi'(0) = \varphi_0' \text{ (given)} \tag{B8b}$$

Integration of equation (B7), with the boundary conditions noted in equation (B8), yields

$$\varphi' = \pm\frac{4}{3}\sqrt{\sqrt{\varphi} - \left[1 - \frac{9}{16}(\varphi_0')^2\right]} \tag{B9}$$

Two types of solutions are possible depending on whether the constant in the brackets of equation (B9) is nonnegative or negative. The two cases are termed type C and type D flows, respectively (in approximate accordance with the notation of refs. 11 and 12). Thus, introduce the nonnegative parameters φ^* and β such that

$$\left[1 - \frac{9}{16}(\varphi_0')^2\right] \equiv \sqrt{\varphi^*} \geq 0 \qquad \text{Type C} \tag{B10a}$$

$$\left[1 - \frac{9}{16}(\varphi_0')^2\right] \equiv -\sqrt{\beta} < 0 \qquad \text{Type D} \tag{B10b}$$

These parameters can now be used instead of φ_0'. Note that $\varphi' = 0$ when $\varphi = \varphi^*$ (from eqs. (B9) and (B10a)). The corresponding value of ξ is denoted by ξ^*. Hence, type C integral curves are characterized by the fact that there is a point (ξ^*, φ^*) on the curve of φ against

ξ at which $\varphi' = 0$. There is no such critical point on the type D integral curves.[1]

Equation (B9) can be integrated to find analytic expressions for the type C and D integral curves. These curves are discussed separately.

Type C Curves

Substituting φ^* into equation (B9) and integrating between the points (ξ^*, φ^*) and (ξ, φ) yield

$$\xi - \xi^* = \pm(\sqrt{\varphi} + 2\sqrt{\varphi^*})\sqrt{\sqrt{\varphi} - \sqrt{\varphi^*}} \qquad \xi \gtrless \xi^* \qquad \text{(B11a)}$$

where (since $\varphi = 1$ when $\xi = 0$)

$$\xi^* = \pm(1 + 2\sqrt{\varphi^*})\sqrt{1 - \sqrt{\varphi^*}} \qquad \varphi_0' \lessgtr 0 \qquad \text{(B11b)}$$

Typical type C curves (characterized by the parameter φ^*) are presented in figure 2 for $\xi \geq 0$. The curves for $\xi < 0$ are the mirror image of those for $\xi > 0$. Curve a, in figure 2, is the envelope of the type C curves. The integral curve corresponding to a given value of φ^* is drawn as a solid line for the portion upstream of its tangency point with curve a and is drawn as a dash-dot-dash line for the downstream portion. The reason for this distinction will be noted presently.

The equation of curve a is found by eliminating ξ^* in equation (B11a) (using eq. (B11b)) and maximizing ξ with respect to φ^* holding φ constant. The result is

$$\left.\begin{aligned} \xi &= (1 + \sqrt{\varphi})^{3/2} \\ &\equiv \xi_a(\varphi) \end{aligned}\right\} \qquad \text{(B12)}$$

The point of tangency for a given type C curve with curve a is found from

$$\left.\begin{aligned} \varphi^* &= \varphi/(1 + \sqrt{\varphi})^2 \\ \text{or} \qquad & \\ \varphi &= \varphi^*/(1 - \sqrt{\varphi^*})^2 \end{aligned}\right\} \qquad \text{(B13)}$$

---

[1]This classification of type C and D curves is consistent with references 11 and 12 with one exception. Integral curves for which ξ^* is negative are included among type C curves herein and are included among the type D curves (characterized by a parameter α) in references 11 and 12.

Curve b, in figure 2, is the right-hand branch of the $\varphi^* = 0$ curve and has the equation (from eq. (B11a) with $\xi^* = 1$, $\varphi^* = 0$)

$$\left.\begin{aligned} \xi &= 1 + \varphi^{3/4} \\ &\equiv \xi_b(\varphi) \end{aligned}\right\} \tag{B14}$$

Curve d is the locus of the critical points on the type C integral curves and is given by (from eq. (B11b))

$$\left.\begin{aligned} \xi &= (1 + 2\sqrt{\varphi})\sqrt{1 - \sqrt{\varphi}} \\ &\equiv \xi_d(\varphi) \end{aligned}\right\} \tag{B15}$$

The region bounded by curves a and b is one for which φ^* is a double-valued function of (ξ,φ). That is, two type C curves pass through each point of this region. (Curve b is included but curve a is excluded from this region of double-valuedness.) The circled point in figure 2 is an example. Both the $\varphi^* = 0.1$ and the $\varphi^* = 0.4$ integral curves pass through this point. Note that at the circled point the $\varphi^* = 0.4$ curve is solid (i.e., it is upstream of its tangent point with curve a), while the $\varphi^* = 0.1$ curve is a dash-dot-dash line (i.e., it is downstream of its tangent point with curve a). Reference 11 has shown that if continuous changes in operating conditions (say, in current) are made for a given one-dimensional electrode configuration, starting from boundary conditions for which the flow is unique, then operation in the double-valued region between curves a and b will always correspond to the curve with the larger value of φ^*. That is, operation will be along the solid lines in figure 2, and not along the dash-dot-dash lines. (The latter are termed type C overlap curves in ref. 11.) Further discussion of the lack of uniqueness of one-dimensional beam flows is given in appendix C.

Type D Curves

Substituting equation (B10b) into (B9) and integrating between the limits (ξ,φ) and $(0,1)$ yield

$$\xi = \pm(\sqrt{\varphi} - 2\sqrt{\beta})\sqrt{\sqrt{\varphi} + \sqrt{\beta}} \mp (1 - 2\sqrt{\beta})\sqrt{1 + \sqrt{\beta}} \qquad \left(\varphi_0' \begin{matrix} > 4/3 \\ < -4/3 \end{matrix}\right) \tag{B16}$$

These curves are also plotted in figure 2 for several values of β and $\xi \geq 0$. For $\varphi_0' < -4/3$, each type D curve terminates at $\varphi = 0$, where $\varphi' = \pm \frac{4}{3}\beta^{1/4}$.

Electric Field and Velocity

The electric field at any point on a type C or type D curve is found from (eqs. (B2), (B5), (B9), and (B10))

$$\left.\begin{aligned} \frac{E}{-V_0/L} &= \pm \frac{4}{3}\sqrt{\frac{j}{j_M}}\sqrt{\sqrt{\varphi} - \sqrt{\varphi^*}} && \text{Type C} \\ &= \pm \frac{4}{3}\sqrt{\frac{j}{j_M}}\sqrt{\sqrt{\varphi} + \sqrt{\beta}} && \text{Type D} \end{aligned}\right\} \quad \text{(B17a)}$$

for $\varphi' \gtrless 0$. The velocity is (eqs. (B3) and (B5a))

$$v = \sqrt{-2\eta V_0 \varphi} \quad \text{(B17b)}$$

APPENDIX C

ONE-DIMENSIONAL CHARGED BEAM WITH CURRENT REVERSAL

In appendix B, one-dimensional single-species charged beam flows were considered wherein the particles all moved in the +x direction. It was found that no integral curves existed downstream of curve a in figure 2. It is now assumed that current reversal occurs at some station in the beam so that two-way currents exist upstream of this station. Such flows, termed type B flows in reference 11, will be shown to have integral curves that fall downstream of curve a in figure 2. In addition, an ion-rocket configuration will be considered where the neutralizing grid is sufficiently far downstream of the accelerating grid to induce ion current reversal between these two grids. The variation of the transmitted ion current with neutralizing-grid voltage and the possibility of hysteresis effects and instability will be noted. The latter discussion will require that no electrons be present between the accelerating and neutralizing grids and is applicable only when (1) the neutralizing grid is not emitting electrons (as may occur in the laboratory in the course of an experimental development program), or (2) electrons are prevented from moving upstream of the neutralizing grid (such as by using separate deceleration and neutralization grids with the latter at a higher voltage than the former).

Assume a current j_e is emitted at some grid and moves in the +x direction. Because of downstream boundary conditions, a virtual grid is assumed to exist such that part (j_r) of the current reverses and part (j_t) is transmitted through the virtual grid (see sketch (d)).

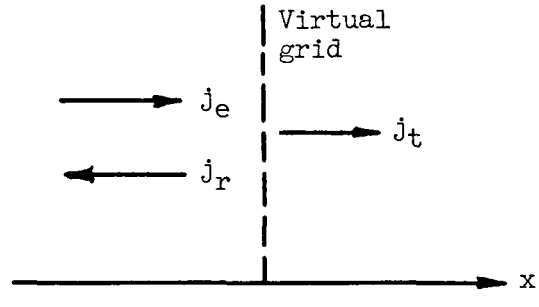

(d)

For ions, j_e and j_t are positive quantities while j_r is negative. From continuity,

$$j_e = j_t + (-j_r) \tag{C1}$$

Assuming the charged particles to have been emitted with zero velocity at zero voltage, the velocity at any point is

$$v = \pm \sqrt{-2\eta V} \tag{C2}$$

where the negative sign is used for the reflected particles. The total charge density upstream of the virtual grid is then

$$\rho_q = \frac{j_e}{\sqrt{-2\eta V}} + \frac{j_r}{-\sqrt{-2\eta V}}$$

$$= \frac{j_e + (-j_r)}{\sqrt{-2\eta V}} \equiv \frac{j_{tot}}{\sqrt{-2\eta V}} \tag{C3}$$

where $j_{tot} \equiv j_e + (-j_r)$ is the sum of the magnitudes of the emitted and reflected currents. Poisson's equation for the region upstream of the virtual grid then becomes

$$\frac{d^2V}{dx^2} = \frac{-j_{tot}}{\epsilon_0\sqrt{-2\eta V}} \tag{C4a}$$

Similarly, Poisson's equation for the downstream region of the virtual grid is

$$\frac{d^2V}{dx^2} = \frac{-j_t}{\epsilon_0\sqrt{-2\eta V}} \tag{C4b}$$

Integration of equations (C4), with suitable boundary conditions, defines the flow upstream and downstream of the virtual grid.

As in the body of the report, consider an emitter at x_e and an accelerating grid at $x = 0$ with a spacing L and voltage difference V_0. A virtual grid is assumed downstream of $x = 0$ (see sketch (e)).

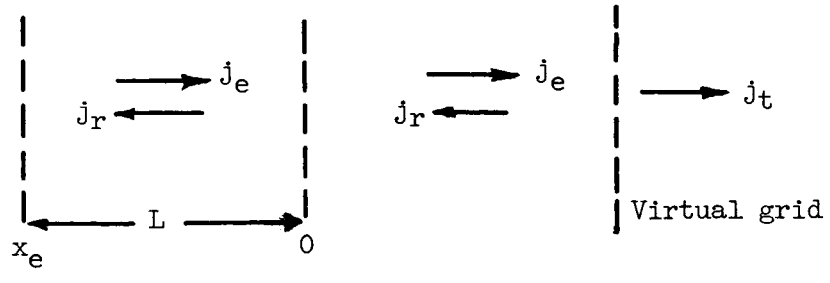

(e)

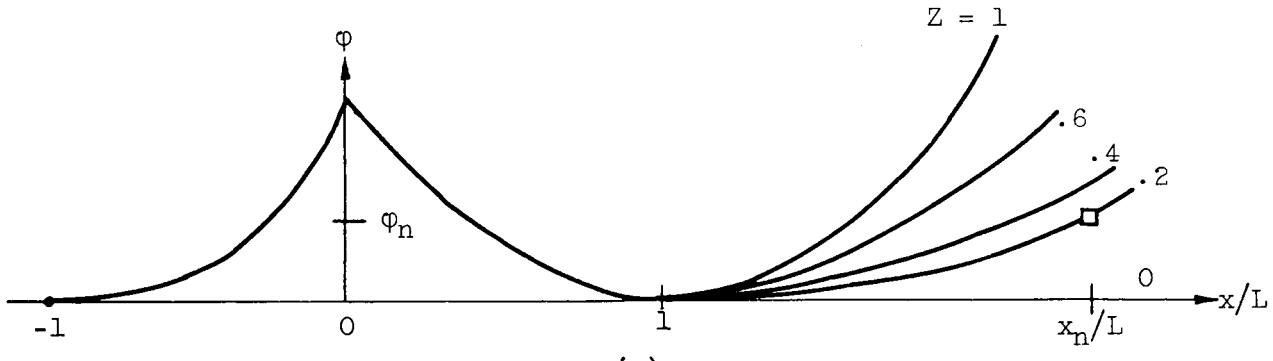

(f)

Assume that the emitter is space-charge-limited so that, at x_e,

$$\varphi = \frac{d\varphi}{dx} = 0 \tag{C5}$$

where $\varphi = V/V_0$. Integration of equation (C4a) with the boundary conditions given by equation (C5) and $\varphi = 1$ at $x = 0$ shows (for $-1 \leq x/L < 0$)

$$\frac{x}{L} = -(1 - \varphi^{3/4}) \tag{C6a}$$

$$j_{tot} = j_M = -\frac{4}{9}\epsilon_0\sqrt{-2\eta V_0}\,\frac{V_0}{L^2} \tag{C6b}$$

This is the Child's law result previously obtained (eq. (3)), except that the current $j_{tot} = j_M$ is the sum of downstream (j_e) and upstream ($-j_r$) moving currents.

At the virtual grid the velocity and electric field are each zero so that the boundary conditions are given by equation (C5). Integration of equation (C4a) then gives (for $0 < \frac{x}{L} < 1$)

$$\frac{x}{L} = 1 - \varphi^{3/4} \tag{C7}$$

showing that the virtual grid is at $x = L$. Equation (C7) is the mirror image of equation (C6a) (see sketch (f)) and is again Child's law.

To find the flow downstream of $x = L$, equation (C4b) is integrated with the boundary conditions $\varphi = \frac{d\varphi}{dx} = 0$ at $x = L$, and the result is (for $x/L > 1$)

$$\left(\frac{x}{L} - 1\right)\sqrt{\frac{j_t}{j_{tot}}} = \varphi^{3/4} \tag{C8}$$

Let Z be the ratio of the transmitted to the emitted current

$$Z = \frac{j_t}{j_e} \tag{C9a}$$

Then, from equation (C1) and the definition of j_{tot},

$$\frac{-j_r}{j_e} = 1 - Z \qquad \frac{j_{tot}}{j_e} = 2 - Z \qquad \frac{j_t}{j_{tot}} = \frac{Z}{2 - Z} \tag{C9b}$$

Equation (C8) can then be written

$$\frac{x}{L} = 1 + \sqrt{\frac{2 - Z}{Z}}\, \varphi^{3/4} \tag{C10}$$

Plots of equation (C10), for various values of Z, are indicated in sketch (f) and in figure 3. These curves differ in appearance from those in figure 2 of reference 11, since the abscissa in the latter figure is $(x/L)\sqrt{j_e/j_M}$.

For a given emitter and accelerator, the transmitted current will depend on the location and voltage of the neutralizing grid. (Substitution of x_n and φ_n into eq. (C10) defines Z and therefore j_t.) Thus $Z = 0.2$ for the values of φ_n and x_n indicated by the square data point in sketch (f).

The type B curves represent a valid description of the flow between the accelerating and neutralizing grids of an ion rocket if the neutralizing grid is not emitting electrons. If electrons are emitted they will be attracted upstream and will modify the flow. A particular solution of a mixed ion-electron beam, upstream of the neutralizing grid, is presented in the body of the report.

Figures 2 and 3 indicate that, when the ion emitter of an ion rocket is space-charge-limited ($j_{tot} = j_M$), three different integral curves pass through each point in the region between curves a and b (assuming no electrons, from the neutralizing grid, are present). Two are type C curves (one of which is a type C overlap curve), and the third is a type B curve. If the neutralizing grid operates in the region between curves a and b, discontinuous changes in transmitted current may occur as the neutralizing-grid potential is varied. This is now discussed (following refs. 11 and 12).

Consider a neutralizing grid to be located at x_n as indicated in figures 4(a) and (b). The emitter is assumed to be space-charge-limited. When φ_n equals $\varphi_{n,1}$ (point 1 in fig. 4), only one integral curve is

possible ($\varphi^* = \varphi_1^*$), and all the current is transmitted (i.e., $j_t/j_M = 1$ in fig. 4(c)). When φ_n is decreased to $\varphi_{n,2}$, two type C curves are possible, either the type C $\varphi^* = \varphi_2^*$ curve or the type C overlap curve $\varphi^* = 0$ (whose branch downstream of $x/L = 1$ is curve b). In either case all current is still transmitted. If the integral curves are assumed to vary continuously (when possible) as φ_n is decreased, then operation will be along $\varphi^* = \varphi_2^*$. Similarly, as φ_n is reduced to $\varphi_{n,3}$, operation will then be along $\varphi^* = \varphi_3^*$ rather than along the type C overlap curve through point 3. Further reduction of φ_n to $\varphi_{n,4}$ results in operation along $\varphi^* = \varphi_4^*$. Since point 4 is on curve a, $\varphi_{n,4}$ is the lowest value of φ_n for which operation along a type C curve is possible. An infinitesimal decrease in φ_n causes the integral curve to shift discontinuously to a type B curve (indicated by $Z = Z_4$ in fig. 4(a)), and only part of the emitted current is transmitted (see fig. 4(c)). Further decreases in φ_n to $\varphi_{n,5}$, $\varphi_{n,6}$, and $\varphi_{n,7} = 0$ result in operation along the type B curves Z_5, Z_6, and $Z_7 = 0$. The corresponding variation in j_t is indicated in figure 4(c).

Now consider the sequence as φ_n is increased from $\varphi_{n,7} = 0$ to $\varphi_{n,2}$. Again assuming that the integral curves vary continuously (when possible) as φ_n increases, then operation will be along the type B curves defined by Z_7 to Z_2, respectively. The transmitted current increases continuously until $j_t/j_M = 1$ at point 2 (fig. 4(c)). As φ_n increases above $\varphi_{n,2}$, a discontinuous change from type B to type C curves occurs with $j_t = j_M$.

Figure 4(c) indicates a hysteresis loop in the variation of j_t/j_M with φ_n. The upper branch of the hysteresis loop corresponds to type C operation, while the lower branch corresponds to type B operation. With decreasing φ_n, the change from type C to type B operation occurs discontinuously at curve a. With increasing φ_n, the change from type B to type C occurs discontinuously at curve b. The validity of the assumption that the integral curves vary continuously, when possible, as φ_n is varied, requires that operation along type B and type C curves is stable (with respect to small disturbances). Otherwise there may be discontinuous changes from type B to type C (including overlap) operation, and vice versa, for any value of φ_n in the range $\varphi_a(x_n) \leq \varphi_n \leq \varphi_b(x_n)$.

If electrons are emitted at ξ_n, the flow in the region $0 < \xi < \xi_n$ will probably correspond to that indicated in figure 5(b) (as discussed in the body of the report).

E-13

APPENDIX D

MOMENTUM-INTEGRAL METHOD FOR THRUST EVALUATION

The thrust of jet engines is often evaluated by applying an integral form of the law of conservation of momentum, the thrust of the engine being related to the flux of momentum and surface stresses at an arbitrary control surface enclosing the engine. When applying this method to ion-rocket engines it is necessary to consider electromagnetic surface stresses as well as fluid surface stresses. Although the appropriate form of the momentum conservation law, including these stresses, is well known in magnetohydrodynamic studies (e.g., ref. 14) the specific application to ion engines does not seem to have been discussed explicitly in the current literature. Therefore, such a discussion is undertaken herein. In particular, the integral form of the law of conservation of momentum is derived for flows of charged particles in the presence of electric and magnetic fields. The resulting expression is then applied to find the thrust of a one-dimensional ion rocket. Local properties are assumed independent of time; mks units are used.

Let S be a simple closed surface, fixed in space, and let $\mathscr{V}$ be the enclosed volume (sketch (g)). The law of conservation of momentum

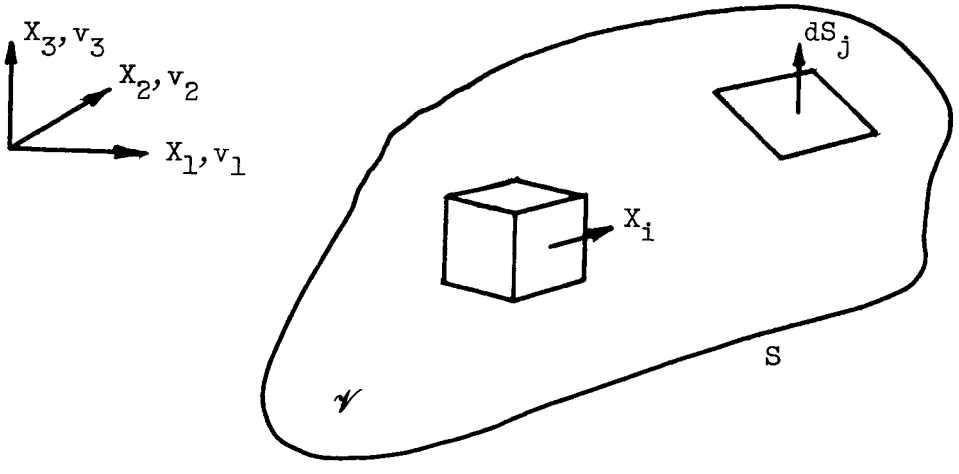

(g)

can be written

$$\int_S \rho_m v_i v_j \, dS_j = \int_{\mathscr{V}} X_i \, d\mathscr{V} \qquad \text{(D1)}$$

assuming steady state, neglecting random thermal motion, and assuming that all particles have the same local properties (mass, velocity, charge) at each point in the flow.[2] Cartesian tensor notation is used. Repeated indices are summed. The left side of equation (D1) gives the net rate of increase of the momentum of the particles entering and leaving S. The term on the right side is the net electromagnetic body force acting on the particles within $\mathscr{V}$ (gravitational forces are neglected). The electromagnetic body force per unit volume X_i can be expressed as the divergence of the Maxwell stress tensor (ref. 15). Thus (for steady state),

$$X_i = \frac{\partial T_{ji}}{\partial x_j} \tag{D2}$$

where

$$T_{ji} = E_j D_i + H_j B_i - \frac{1}{2}\delta_{ij}(E_k D_k + H_k B_k)$$

Substituting equation (D2) into equation (D1) and applying the divergence theorem (assuming X_i is regular in $\mathscr{V}$) yield

$$\int_S \rho_m v_i v_j \, dS_j = \int_S T_{ji} \, dS_j \tag{D3}$$

which is an alternative form of the law of conservation of momentum.

Equation (D3) can be used to find the net force on an arbitrary body in the presence of charged particles and electromagnetic fields. Let the control surface S consist of three parts, namely, an arbitrary surface enclosing the body (S'), a surface taken directly about the body (S"), and a slit (S''') which connects S' to S". The slit S'''

---

[2]For a multiple-specie stream of particles, with N distinct species, the integrands in equation (D1) represent the sums

$$\rho_m v_i v_j \equiv \sum_{r=1}^{N} (\rho_m v_i v_j)_r$$

$$X_i \equiv \sum_{r=1}^{N} (X_i)_r$$

where $(\rho_m v_i v_j)_r$ and $(X_i)_r$ are the values for the r^{th} specie. Similar summations are required if the particles have thermal motion. An alternative approach, in the case of thermal motion, is to let ρ_m, v_i, and X_i represent local mean values (suitably defined) and introduce a fluid surface stress tensor into equation (D1) (e.g., ref. 14).

excludes the body from the interior of S' (sketch (h)), thereby assuring the regularity of X_i in $\mathscr{V}$ and permitting application of the

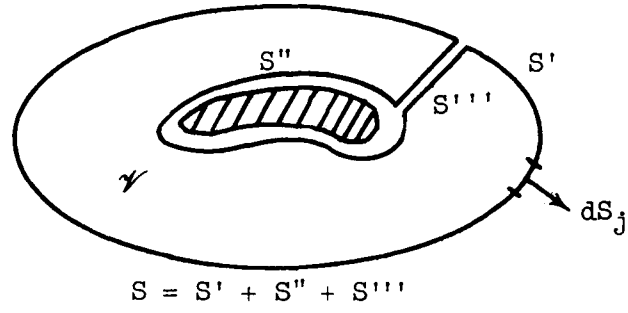

(h)

divergence theorem. Evaluating equation (D3) for the surface $S = S' + S'' + S'''$ gives

$$\int_{S'+S''} \rho_m v_i v_j \bar{dS}_j = \int_{S'+S''} T_{ji}\, dS_j \qquad \text{(D4)}$$

(The net contribution of the slit S''' is zero.) But, the net force exerted on the body, denoted by F_i, can be expressed as

$$F_i \equiv - \int_{S''} (T_{ji} - \rho_m v_i v_j) dS_j$$

where the minus sign is required because here dS_j is an inward normal with respect to the body surface (sketch (h)). In the latter expression the T_{ji} term represents the electromagnetic surface stresses on the body, and the $\rho_m v_i v_j$ term is the reaction if particles impinge on or are emitted at the surface. The net force on the body can then be found by the following surface integration about S' (from eq. (D4)):

$$F_i = \int_{S'} (T_{ji} - \rho_m v_i v_j)\, dS_j \qquad \text{(D5)}$$

Thus the net force can be found by integrating the surface stresses and the momentum flux about an arbitrary surface S' enclosing the body.

For an ion rocket that does not employ magnetic fields, the magnetic-field terms in equation (D2) can be neglected.[3] Also, $D_i = \epsilon_0 E_i$, so that T_{ji} becomes

$$T_{ji} = \epsilon_0 \left(E_i E_j - \frac{\delta_{ij}}{2} E_k E_k \right) \tag{D6}$$

It can be shown (e.g., ref. 15) that the resultant surface force, $T_{ij}\, dS_j$, on a surface element dS_j, associated with a local electric field E_i, is such that E_i bisects the angle between $T_{ij}\, dS_j$ and

[3]It can be shown that the self-induced magnetic field, associated with an ion beam of finite width, is negligible. Consider an ion beam of radius R undergoing a Child's law acceleration through a length L and voltage difference V_0 (sketch (i)). Characteristic quantities are $E_i \sim V_0/L$,

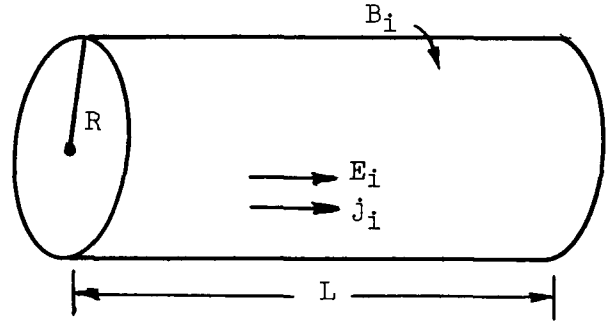

(i)

$v_i \sim \sqrt{-\eta V_0}$, $j_i = \rho_q v_i \sim \epsilon_0 \sqrt{\eta} V_0^{3/2} / L^2$. The characteristic magnetic field at the edge of the beam is $B_i \sim \mu_0 j_i R$, which follows from Maxwell's equation $\overline{\nabla} \times \overline{B} = \mu_0 \overline{j}$. The ratio of the magnetic-field force to the electric-field force at the edge of the beam is then

$$\frac{(F)_{mag}}{(F)_{elec}} \equiv \frac{\rho_q \overline{v} \times \overline{B}}{\rho_q \overline{E}} \sim \frac{v_i B_i}{E_i} \sim \frac{v_i^2}{c^2} \frac{R}{L}$$

where $c^2 \equiv 1/\mu_0 \epsilon_0$ is the square of the speed of light. For specific impulses and geometries of current interest, the induced magnetic-field effects are negligible.

dS_j (sketch (j)). Thus, if E_i is normal to the surface, the resultant force is a tension regardless of the direction of E_i (sketches (k) and (m)). If E_i is parallel to the surface, the resultant force is a compression (sketch (l)).

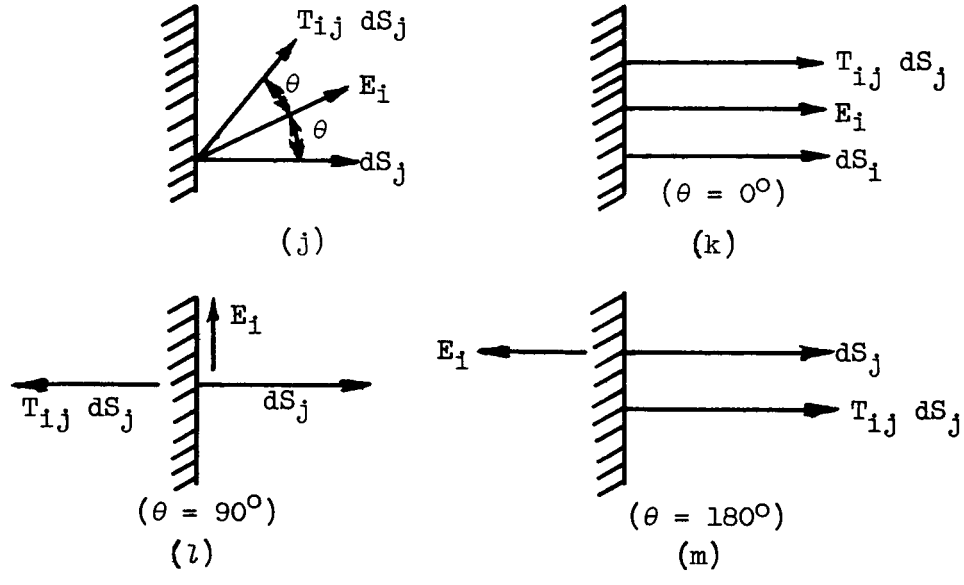

Substitution of equation (D6) into (D5) gives

$$F_i = \int_{S'} \left[\epsilon_0 \left(E_i E_j - \frac{\delta_{ij}}{2} E_k E_k \right) - \rho_m v_i v_j \right] dS_j \qquad \text{(D7)}$$

For a one-dimensional beam ($E_1 \neq 0$, $v_1 \neq 0$, $E_2 = E_3 = v_2 = v_3 = H_i = 0$), the force exerted by the fluid between stations $(x_1)_\alpha$ and $(x_1)_\beta$ is

$$f_i = \left[\frac{\epsilon_0 E_1^2}{2} - \rho_m v_1^2 \right]_{(x_1)_\alpha}^{(x_1)_\beta} \qquad \text{(D8)}$$

where f_1 is the force per unit cross-sectional area, and $(x_1)_\beta > (x_1)_\alpha$. The term $\rho_m v_1^2$ represents the local flux of momentum,[4] while $\epsilon_0 E_1^2/2$ represents a tensive surface force, as noted in connection with sketches (k) and (m). Thus, $-\epsilon_0 E_1^2/2$ is a compressive surface force and

[4]For a multiple-specie flow $\rho_m v_1^2$ represents the total flux of momentum (e.g., footnote 2). This term equals twice the local kinetic energy for the present case of one-dimensional flow.

corresponds to the pressure term, p, in ordinary one-dimensional fluid mechanics. The subscript 1 is superfluous for strictly one-dimensional flows and is henceforth omitted.

It is instructive to find an integral of equation (B1). Combining equations (B1b) and (B1c) gives

$$\epsilon_0 E \frac{dE}{dx} - \frac{j}{\eta} \frac{dv}{dx} = 0 \tag{D9}$$

Integrating,

$$\epsilon_0 \frac{E^2}{2} - \frac{j}{\eta} v = \text{const} \tag{D10a}$$

or

$$\epsilon_0 \frac{E^2}{2} - \rho_m v^2 = \text{const} \tag{D10b}$$

Comparison of equation (D10b) with equation (D8) shows that no thrust force is developed between two points on a single integral curve satisfying equation (B1). However, if grids are permitted, thrust can be developed; and the thrust arises, in fact, from forces on these grids.

The force on a grid is most easily evaluated by taking x_α and x_β to be an infinitesimal distance upstream and downstream of the grid, respectively. Thus, the force on a grid at x_g is

$$(f)_{x_g} = \lim_{\epsilon'' \to 0} \left[\frac{\epsilon_0 E^2}{2} - \rho_m v^2 \right]_{x_g - \epsilon''}^{x_g + \epsilon''} \tag{D11}$$

If no particles impinge on or originate at the grid, then $\rho_m v^2$ is a continuous function of x near x_g (since the potential V is a continuous function of x), and the force on the grid becomes

$$(f)_{x_g} = \lim_{\epsilon'' \to 0} \left[\frac{\epsilon_0 E^2}{2} \right]_{x_g - \epsilon''}^{x_g + \epsilon''} \tag{D12}$$

If particles originate at or impinge on the grid, then the full equation (eq. (D11)) must be used. As an example, consider the force on a conducting "target" due to impingement of an ion beam (sketch (n)).

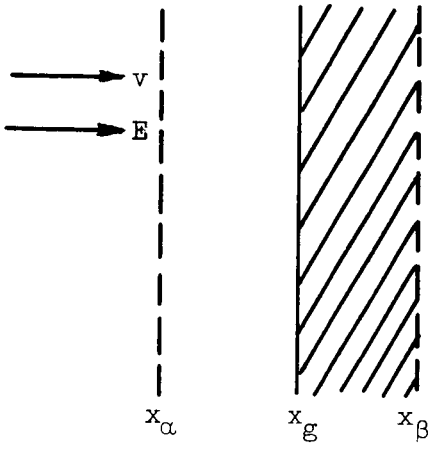

(n)

Station x_β does not contribute, since $E = v = 0$. The force on the target is then

$$(f)_{x_g} = -\left[\frac{\epsilon_0 E^2}{2} - \rho_m v^2\right]_{x_\alpha}$$

$$= -\lim_{\epsilon'' \to 0}\left[\frac{\epsilon_0 E^2}{2} - \rho_m v^2\right]_{x_g - \epsilon''} \qquad \text{(D13)}$$

Both the local electric field and the local flux of momentum contribute to $(f)_{x_g}$. Such a target can be used to measure the thrust of an ion rocket. The force on the target is equal and opposite to the ion-rocket thrust, if particles are not emitted (from the target) with significant momentum in the x direction.

Equations (D8) and (D12) are used in the body of the report to compute the overall thrust and the thrust force on the grids of an ion rocket.

REFERENCES

1. Moeckel, W. E.: Propulsion Methods in Astronautics. Paper presented at Int. Cong. Aero. Sci., Madrid (Spain), Sept. 8-13, 1958.

2. Irving, J. H., and Blum, E. K.: Comparative Performance of Ballistic and Low-Thrust Vehicles for Flight to Mars. Vistas in Astronautics. Vol. II. Pergamon Press, 1959, pp. 127-135; discussion, pp. 135-136.

3. Camac, Morton: Reduction of Flight Time and Propellant Requirements of Satellites with Electric Propulsion by the Use of Stored Electrical Energy. Rep. 36, Avco Res. Lab., Oct. 1958.

4. Childs, J. H.: Design of Ion Rockets and Test Facilities. Paper No. 59-103, Inst. Aero. Sci., 1959.

5. Shook, Gail B.: Ionic Propulsion - An Assessment. Rep. LMSD-48456, Missiles and Space Div., Lockheed Aircraft Corp., Feb. 18, 1959.

6. Langmuir, David B.: Problems of Thrust Production by Electrostatic Fields. Vistas in Astronautics. Vol. II. Pergamon Press, 1959, pp. 191-218; discussion, p. 218.

7. Eilenberg, S. L.: Accelerator Design Techniques for Ion Thrust Devices. R-1430, Rocketdyne, North Am. Aviation, Inc., Feb. 12, 1959. (Contract AF-49(638)-344.)

8. Seitz, Robert N., and Raether, Manfred J.: A Pierce Gun Design for an Accelerate-Decelerate Ionic Thrust Device. Paper presented at ARS meeting, San Diego (Calif.), June 8-11, 1959.

9. Fox, Robert H.: Study of Electric Propulsion Systems for Space Travel. UCRL 5478, Interim Prog. Rep. for July 1 to Dec. 31, 1958, Lawrence Radiation Lab., Univ. Calif., Feb. 6, 1959.

10. Kaufman, Harold R.: One-Dimensional Analysis of Ion Rockets. NASA TN D-261, 1960.

11. Fay, C. E., Samuel, A. L., and Shockley, W.: On the Theory of Space Charge Between Parallel Plane Electrodes. Bell System Tech. Jour., vol. 17, no. 1, Jan. 1938, pp. 49-79.

12. Spangenberg, Karl Ralph: Vacuum Tubes. McGraw-Hill Book Co., Inc., 1948.

13. Child, C. D.: Discharge from Hot Lime. Phys. Rev., vol. 32, 1911, pp. 492-511.

14. Grad, Harold: Notes on Magneto-Hydrodynamics. Pt. I - General Fluid Equations. MH-1, Inst. Mathematical Sci. New York Univ., Aug. 1, 1956.

15. Panofsky, W. K. H., and Phillips, M.: Classical Electricity and Magnetism. Addison-Wesley Publ. Co., Inc., 1955, p. 164.

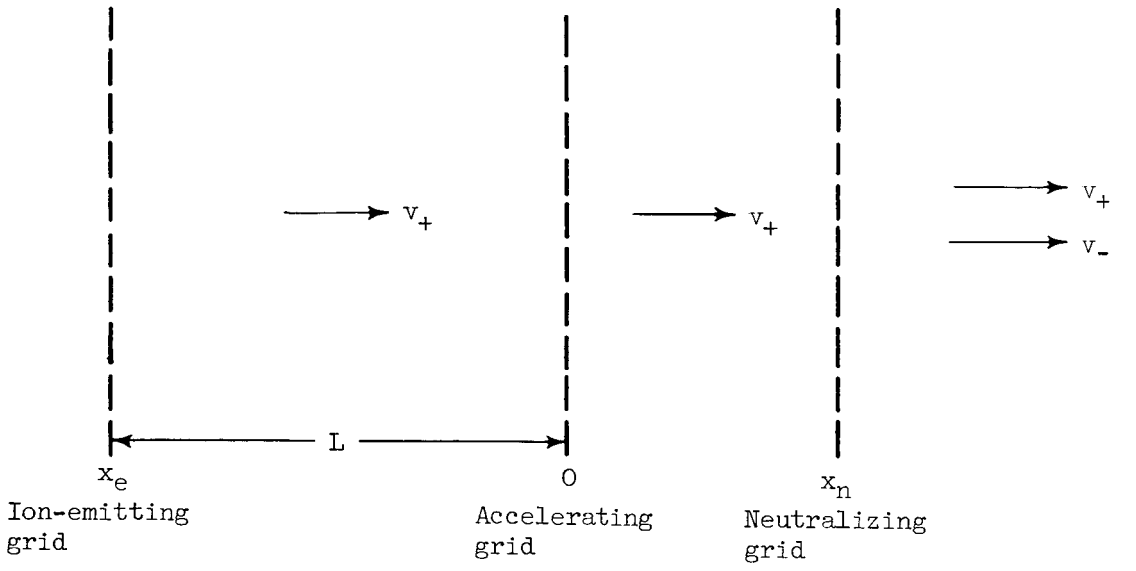

(a) Grid system.

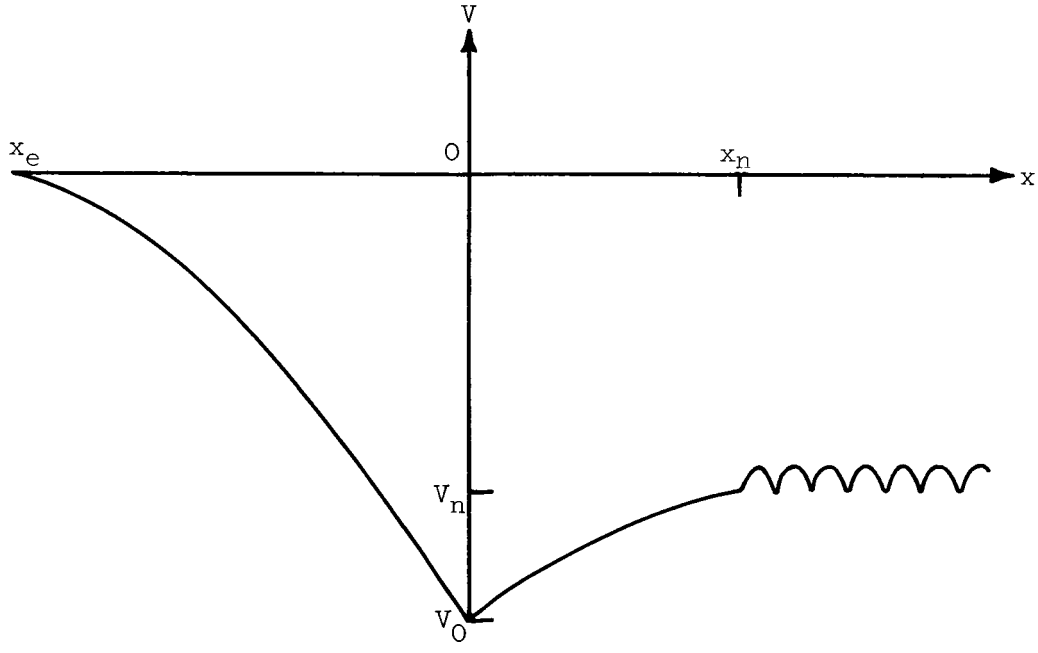

(b) Voltage distribution.

Figure 1. - One-dimensional ion rocket employing accelerate-decelerate cycle. Ions are emitted by grid at x_e and are accelerated by grid at $x = 0$. Grid at x_n decelerates ion beam and emits sufficient electrons to neutralize it.

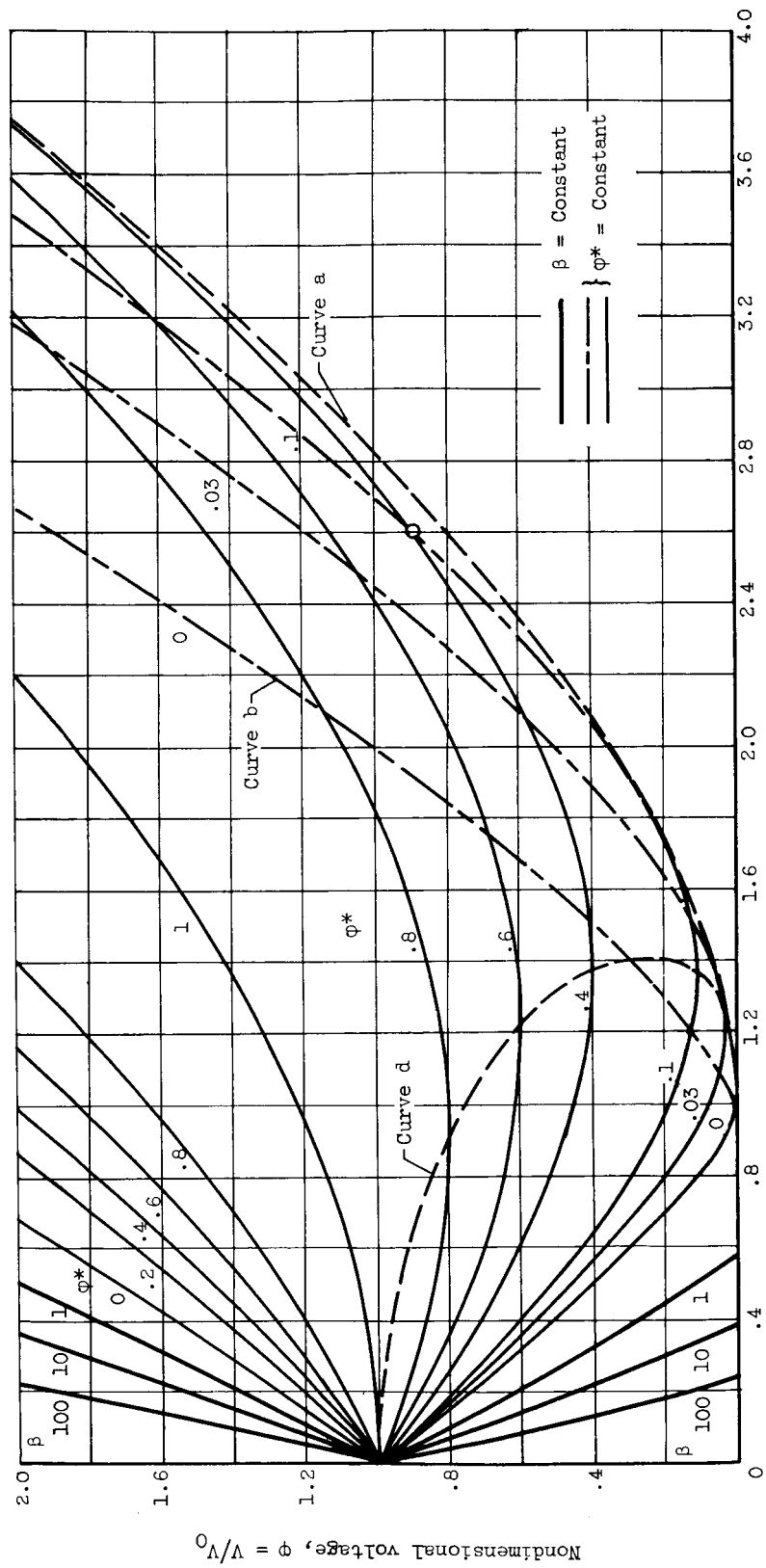

Figure 2. - Type C and D integral curves are characterized by parameters φ^* and β, respectively. Curve a is envelope of type C curves; curve b is downstream branch of $\varphi^* = 0$ curve; curve d is locus of minimum points of type C curves; dash-dot-dash portions of type C curves are called overlap curves.

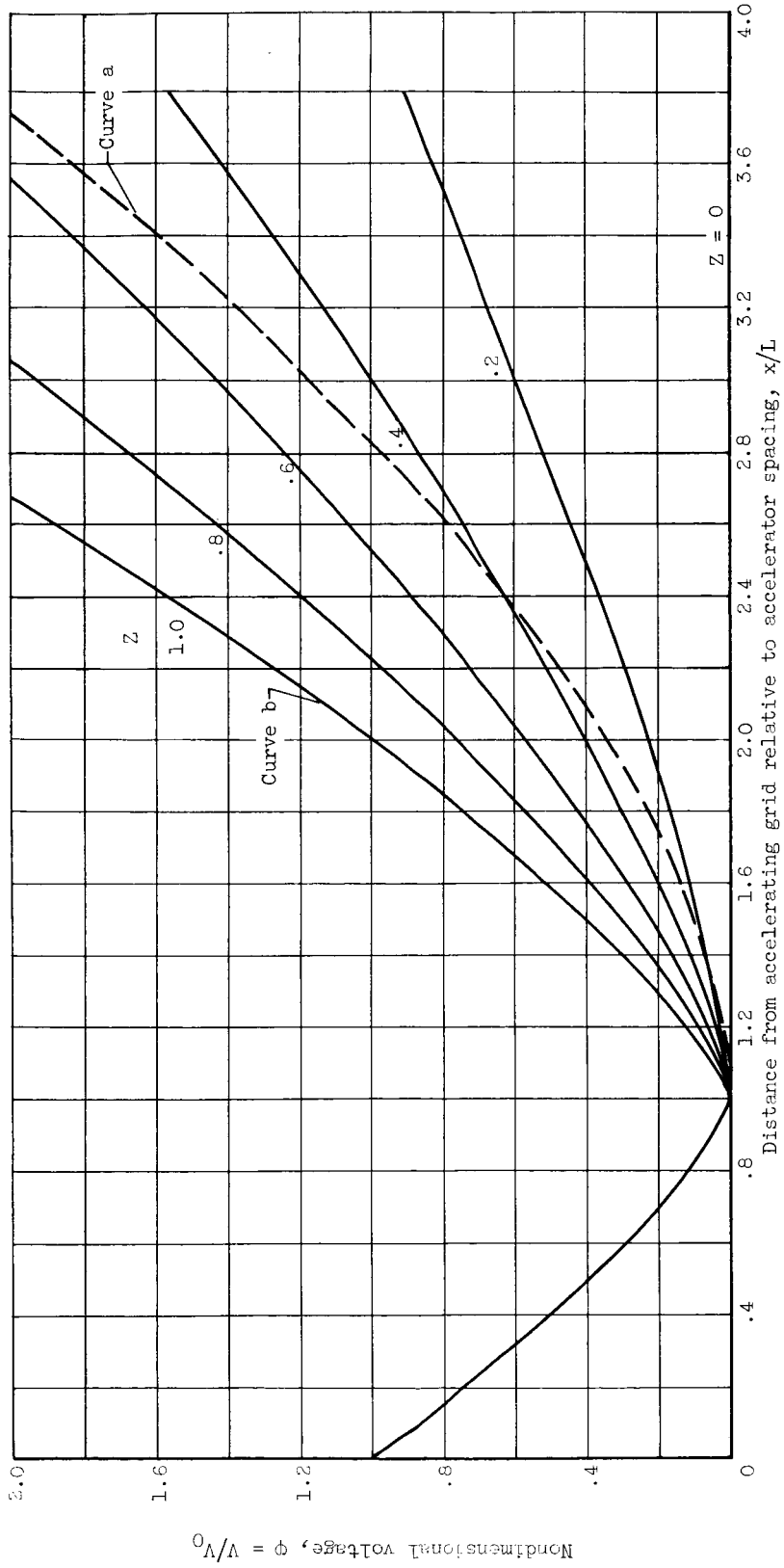

Figure 3. - Type B integral curves for space-charge-limited ion emitter ($j_{tot} = j_M$).

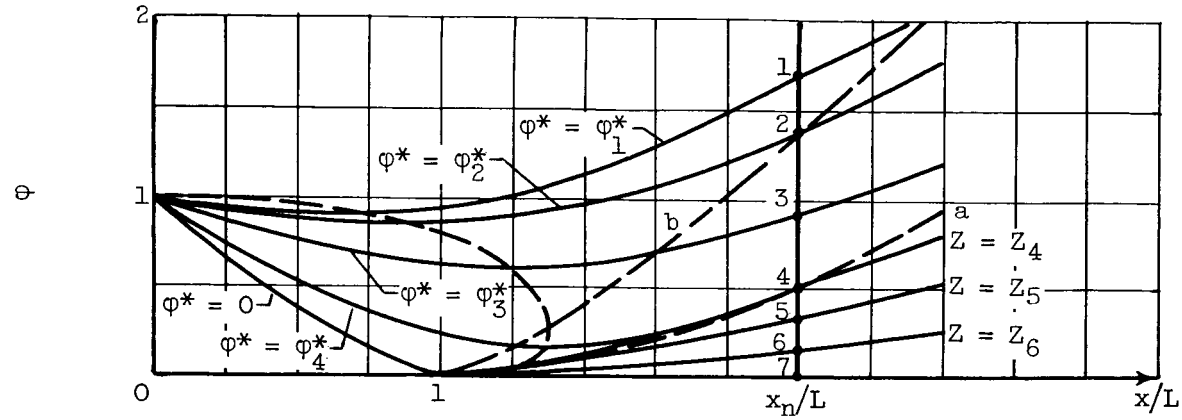

(a) Integral curves as φ_n decreases to zero.

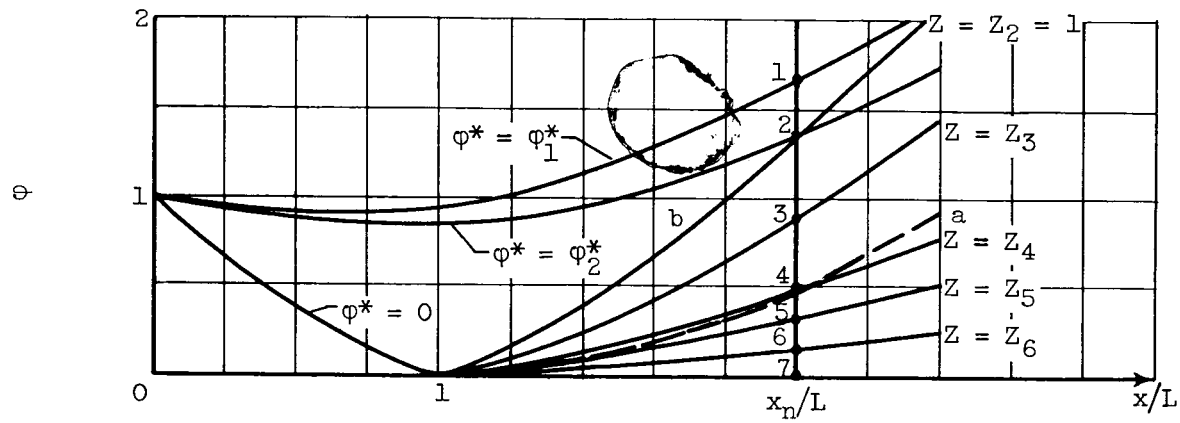

(b) Integral curves as φ_n increases from zero.

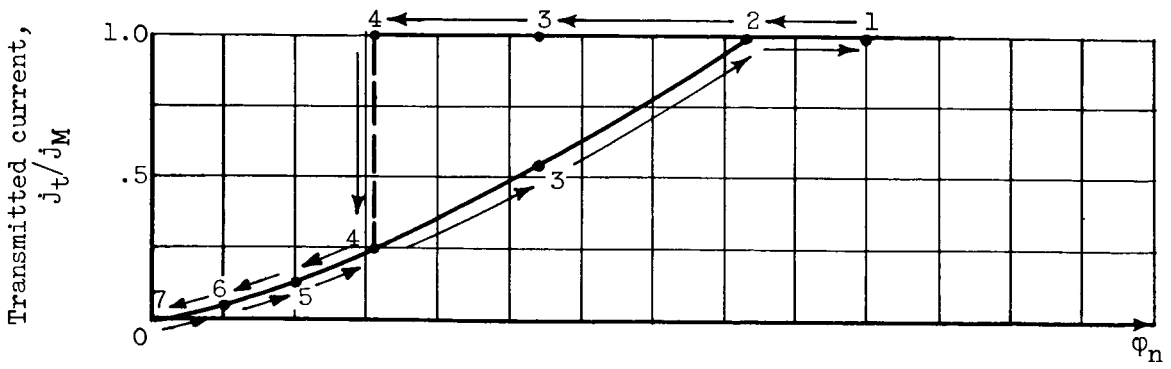

(c) Transmitted current as function of φ_n.

Figure 4. - Illustration of possible hysteresis effects as neutralization grid potential φ_n is varied. It is assumed that ion emitter is space-charge-limited ($j_{tot} = j_M$) and that no electrons are present.

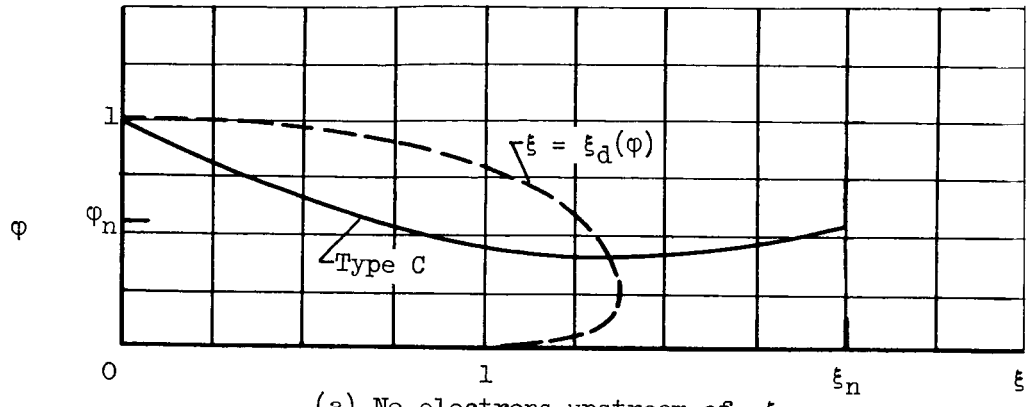

(a) No electrons upstream of ξ_n.

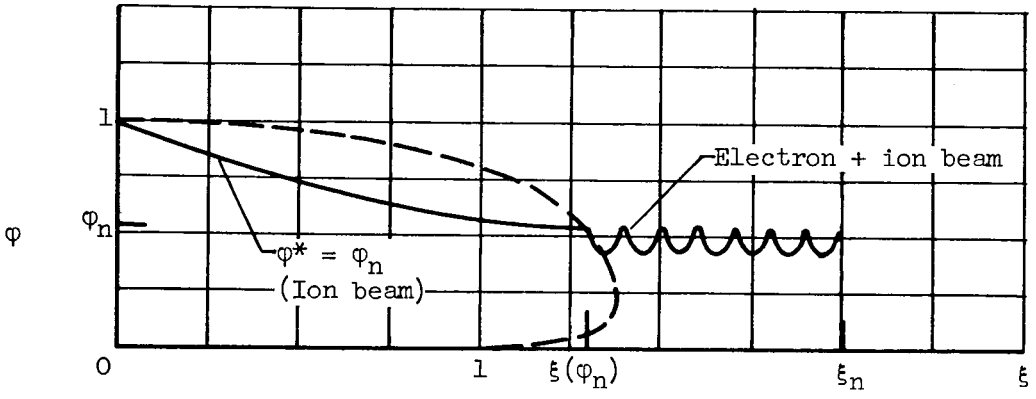

(b) Electrons between $\xi_d(\varphi_n)$ and ξ_n.

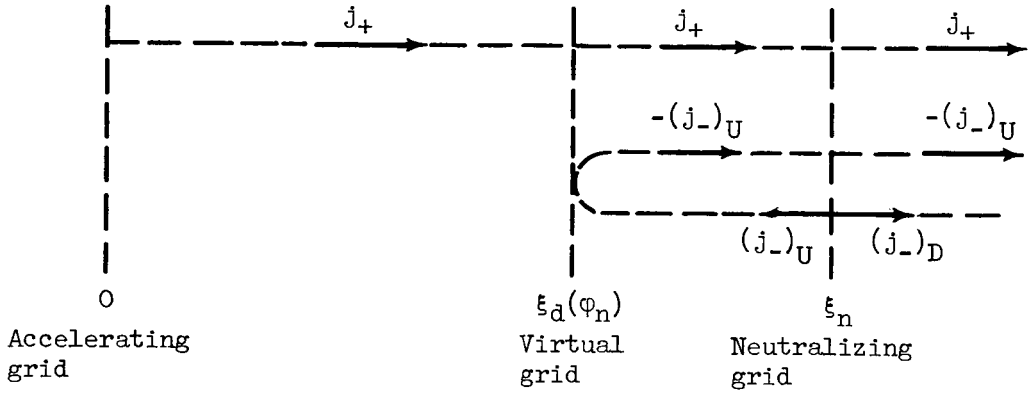

(c) Electron and ion currents corresponding to (b).

Figure 5. - Modification of type C curve in deceleration region ($0 < \xi < \xi_n$) due to presence of electrons from neutralizing grid.